



Article

Long Time-Series Mapping and Change Detection of Coastal Zone Land Use Based on Google Earth Engine and Multi-Source Data Fusion

Dong Chen ^{1,2,†}, Yafei Wang ^{1,2,†}, Zhenyu Shen ^{1,3,*}, Jinfeng Liao ^{1,2}, Jiezhi Chen ⁴ and Shaobo Sun ⁵

¹ Key Laboratory of Regional Sustainable Development Modeling, Institute of Geographic Sciences and Natural Resources Research, Chinese Academy of Sciences, Beijing 100101, China; chend.04b@igsrr.ac.cn (D.C.); wangyafei@igsrr.ac.cn (Y.W.); liaojinfeng21@mails.ucas.ac.cn (J.L.)

² College of Resources and Environment, University of Chinese Academy of Sciences, Beijing 100049, China

³ College of Geographical Sciences, Qinghai Normal University, Xining 810008, China

⁴ College of Land Science and Technology, China Agricultural University, Beijing 100193, China; 2019321010220@cau.edu.cn

⁵ Institute of Surface-Earth System Science, School of Earth System Science, Tianjin University, Tianjin 300072, China; shaobo.sun@tju.edu.cn

* Correspondence: shenzy0921@163.com

† Shared first authorship.

Abstract: Human activities along with climate change have unsustainably changed the land use in coastal zones. This has increased demands and challenges in mapping and change detection of coastal zone land use over long-term periods. Taking the Bohai rim coastal area of China as an example, in this study we proposed a method for the long time-series mapping and change detection of coastal zone land use based on Google Earth Engine (GEE) and multi-source data fusion. To fully consider the characteristics of the coastal zone, we established a land-use function classification system, consisting of cropland, coastal aquaculture ponds (saltern), urban land, rural settlement, other construction lands, forest, grassland, seawater, inland fresh-waters, tidal flats, and unused land. We then applied the random forest algorithm, the optimal classification method using spatial morphology and temporal change logic to map the long-term annual time series and detect changes in the Bohai rim coastal area from 1987 to 2020. Validation shows an overall acceptable average accuracy of 82.30% (76.70–85.60%). Results show that cropland in this region decreased sharply from 1987 (53.97%) to 2020 (37.41%). The lost cropland was mainly transformed into rural settlements, cities, and construction land (port infrastructure). We observed a continuous increase in the reclamation with a stable increase at the beginning followed by a rapid increase from 2003 and a stable intermediate level increase from 2013. We also observed a significant increase in coastal aquaculture ponds (saltern) starting from 1995. Through this case study, we demonstrated the strength of the proposed methods for long time-series mapping and change detection for coastal zones, and these methods support the sustainable monitoring and management of the coastal zone.

Keywords: coastal zone; land use; time series; multi-source data fusion; random forest; classification; change detection; reclamation; aquaculture



Citation: Chen, D.; Wang, Y.; Shen, Z.; Liao, J.; Chen, J.; Sun, S. Long Time-Series Mapping and Change Detection of Coastal Zone Land Use Based on Google Earth Engine and Multi-Source Data Fusion. *Remote Sens.* **2022**, *14*, 1. <https://doi.org/10.3390/rs14010001>

Academic Editor: Sandra Eckert

Received: 16 November 2021

Accepted: 16 December 2021

Published: 21 December 2021

Publisher's Note: MDPI stays neutral with regard to jurisdictional claims in published maps and institutional affiliations.



Copyright: © 2021 by the authors. Licensee MDPI, Basel, Switzerland. This article is an open access article distributed under the terms and conditions of the Creative Commons Attribution (CC BY) license (<https://creativecommons.org/licenses/by/4.0/>).

1. Introduction

About 75% of the world's large cities and 70% of industrial capital and population are concentrated within the 100-km-width coastal zones. Highly concentrated populations and economic activities lead to significant land-use changes in coastal zones [1–3]. Specifically, the rapid expansion of human activities such as off-shore aquaculture, coastal tourism, coastal infrastructure construction, and reclamation has led to great changes in coastal zone land use, triggering a series of ecological and environmental problems such as contamination of the coastal zone environment, massive degradation of wetlands, and destruction of biodiversity and habitats [4,5]. The complicated land-use changes call for remote sensing

technology to monitor land-use changes for sustainable coastal development [6], especially the quick and accurate long time-series and high-density classification mapping and change detection of land use [7–9].

Previous studies of land-use function change detection in traditional coastal zone regions have generally used classification-based change detection methods. At present, there are mainly two kinds of methods; one is the more traditional and commonly used post-classification comparison method, and the other is change detection based on time trajectory analysis. The former is to firstly classify the images based on a single time phase, and then compare the classification results of different time phases to obtain change detection information. The anniversary date or anniversary window (annual cycle or its multiples) is generally introduced. It is mostly used for the overall analysis of all-element land-cover types [10], emphasizing the classification accuracy and algorithm research on single images, and mostly using support vector machines [11], decision trees [12], random forests [13], and various deep learning methods of neural networks [14]. It minimizes discrepancies in reflectance caused by seasonal vegetation fluxes and sun angle differences, allowing rapid access to trending changes between land classes in a particular time period in a region. However, it is prone to overlooking the detailed features in the same. The latter method is to detect temporal sudden change points to obtain the transformation of target features by constructing time-series indices to reconstruct the growth process of features, capitalizing on their seasonal and cyclical characteristics. It mostly targets single land-cover types [15] and focuses more on intra- and inter-annual variation at the time-series scale, such as the convolutional neural network (CNN) model [16], the break for additive season and trend (BFAST) model [17], and the time-series detection methods based on NDVI time-series-derived indexes [18]. These methods are effective in capturing the direction and time of transition between land-cover types and better reflect the shift pattern, but they also require large amounts of calculation. Due to the rapid rate of land surface renewal and complex inter-land class transformation relationships in the coastal zone caused by human activities, it is necessary to combine the advantages of both methods for large-scale, long time-series, and high-frequency land cover classification and change detection.

The recently developed Google Earth Engine (GEE), a cloud platform for geospatial data analysis, provides alternatives for analyzing the long-term and large-area land-use changes [19]. Significant progress has been made in the GEE application for coastal zones, e.g., coastal mudflats [20,21], wetlands [22,23], mangroves [24,25], shorelines [26–28], and coastal development activities such as aquaculture nets [29], aquaculture ponds [30–32], and land reclamation [33,34]. Current studies mainly focus on limited land use in coastal zones, lacking the full-coverage classification of coastal zone land use, especially the sea-land integration [13,35,36]. In particular, the water with the same natural attributes in this area corresponds to different functional attributes, such as seawater, aquaculture ponds, and inland freshwater, respectively corresponding to ecological, production, and living functional attributes. At present, for the extraction research of aquaculture ponds, satellite images with spatial resolution higher than or equal to 10 m are mostly used, including sentinel-1 SAR [37], SPOT5 [38], and gf-2 [39] images. The extraction methods can be divided into a traditional semi-automatic classification based on rules, and automatic classification based on deep learning, which can get good classification results but cannot carry out long-time monitoring research. In addition, people pay more attention to lakes for the extraction of fresh water, and the research area is concentrated in inland areas, with few other types of water interference [40,41]. The sea-land integration requires taking advantage of the multi-source data integration of the big data platform and the insurance on reasonable change logic between time series and spatial neighborhoods, which significantly limits the accuracy of the classification and change detection.

As the largest bay area in China, Bohai rim coastal zone is the most densely populated and economically concentrated area in northern China, as well as one of the key areas with the most drastic land-use changes and the most prominent ecological and environmental problems in China. Previous studies on this region have mostly focused on the detection of

changes in wetlands [21], vegetation [42], shoreline [26,28], land reclamation, and urban expansion [34], while studies on long time-series, high-frequency classification mapping and change detection for solving sustainable development problems caused by human production and life activities using large data of remote sensing images in this region are still limited. Thus, taking the Bohai Sea coastal zone region of China as an example, we proposed a GEE-based land-use function long time-series classification mapping and change detection method for the coastal zone by improving the land-use function classification for human production and life in the coastal area and the integration of sea and land. We explored the combined application of multi-source data fusion, spatial morphological analysis, and logical consistency of spatial and temporal changes in the process. The final analysis of the transformation of coastal land use functions and the characteristics of changes in reclamation construction focused on the salient phenomena of the historical evolution of offshore aquaculture and salt flats and reclamation.

2. Study Area and Datasets

2.1. Study Area

Bohai rim coastal area is located in the northeast of China, from Panshan County in Liaoning Province (north) to Rizhao City in Shandong Province (south) ($35^{\circ}5' \sim 41^{\circ}27' \text{ N}$, $116^{\circ}42' \sim 125^{\circ}41' \text{ E}$), with a coastline of about 6050 km, accounting for one-third of coastline in China [42] (Figure 1). In this study, we focused on 17 coastal cities and 107 coastal districts and counties, with a land area of 154,000 square kilometers across Shandong, Hebei, Liaoning provinces, and Tianjin. The Bohai Sea is the only inland sea in China. It has shallow water, a slow slope, and high nutrient salt content, providing favorable conditions for fisheries. The Yellow River, the Hai River, and the Liao River flow into the sea bringing a lot of sediment, forming a vast area of mudflats and a long natural coastline. The typical landscape of the coastal zone is low-lying plains with a large amount of arable land, covering the southwestern part of the Yellow and Huaihai Plain [3,43]. According to the seventh census data of China, Bohai rim coastal area accommodates nearly 5% of the national population with 1.6% of the national land creating 29.2% national marine GDP. In the past 30 years, driven by the economic growth targets of various local governments along the coast, the expansion of offshore aquaculture, industrial parks, ports, infrastructure, and other construction has been very drastic, and the reclamation activities have been very significant. The excessive encroachment of production and living space on ecological land in the region causes offshore pollution, ecosystem destruction, and continuous reduction of natural shorelines, which is extremely prominent [44].

2.2. Multi-Source Datasets

The historical time-series remote sensing images were selected using the pixel-based mosaic method [45] from Landsat Thematic Mapper (TM), Enhanced Thematic Mapper Plus (ETM+), and Operational Land Imager (OLI) with imaging time between June and October, cloudiness less than 10% for each year from 1987 to 2020. To improve the classification accuracy, we introduced VIIRS nighttime light data (Nighttime Day/Night Band Composites Version 1), digital elevation data (SRTM), spectral indices (normalized vegetation index (NDVI), normalized building index (NDBI)), and multiple water indices to enhance water features in images (normalized difference water index (NDWI), modified normalized difference water index (MNDWI)) [46,47]. We also retrieved the point of interest (POI) big data and the remotely sensed land-use coverage products produced by the Resource and Environment Data Center of the Chinese Academy of Sciences at 5 year intervals for cross-validation and prior knowledge inputs [42].

2.3. Classification System and Sampling

To detect the land-use changes in both sea and land with coastal characteristics, we refined the land-use classification system (Table 1). Specifically, for land reclamation and aquaculture, water was further divided into coastal aquaculture ponds (saltern), inland

fresh-waters and seawater; impervious surfaces into urban land, rural settlement, and other construction lands; and unused areas into tidal flats and unused land.

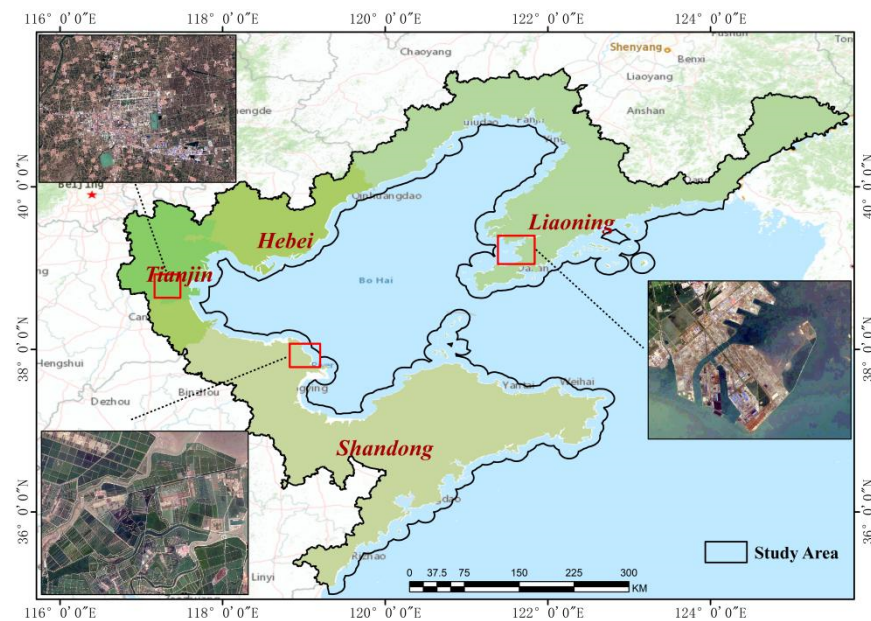


Figure 1. Location of the study area.

Table 1. Coastal zone landscape function classification system.

Class I	Class II	Description
Cropland	-	Refers to land used for growing crops
Grassland	-	Natural grassland and improved grassland
Forest	-	Refers to natural and man-made forests with canopy density >30%
Water	Coastal aquaculture ponds (saltern)	Shallow artificial water bodies with distinctly man-made shape for aquaculture production
	Seawater	Shallow sea within 10 km offshore buffer zone
	Inland fresh-waters	Rivers, ditches, reservoirs, lakes, and other natural water bodies
Impervious surface	Urban land	Land for urban and built-up areas above county level
	Rural settlement	Residential land below county level
	Other construction lands	Independent of factories and mines, large industrial areas, ports, transportation land, airports, and special land outside cities and towns
Other land	Tidal flats	Beaches, salt marshes, and bare land in coastal areas
	Unused land	Land not yet used, including barren land

Samples for training and validation were established based on field trips and manual labels for each year from 1987 to 2020. We conducted a field trip to the study area in 2020 and recorded the field GPS points for each land-use class. To obtain the sample points for 2019, we changed the map to 2019 and checked whether the land-use type of each sample had changed to modify them. By analogy, the whole time-series was traced until 1987, and all sample points were obtained. This sample selection strategy can ensure the overall accuracy and stability of the sample sets. Finally, there were 1300 sample points for primary land-use types, evenly distributed throughout the study area, of which 80% were used

for training and 20% were used for validation. Among the validation samples, 200 were selected for accuracy evaluation for Class I land-use types.

3. Methods

We proposed a framework for the long time-series mapping and change detection of coastal zone land use based on GEE and multi-source data fusion. Firstly, a land-use classification system of coastal zone based on human production, living, and ecology was constructed, and initial classification of long time-series images was carried out using random forest algorithms based on multi-source big data. Secondly, the spatial separation between urban land, rural settlement, other construction lands, and inland fresh-waters, seawater and aquaculture ponds (saltern) was achieved by using the scan line seed filling algorithm and geometric feature analysis, and the functional types involved in cropland transformation, aquaculture ponds (saltern), and reclamation were revised based on the logic rules of spatio-temporal change. Finally, according to the classification results and the results of change nodes, the scope of change and temporal stages of cropland, aquaculture ponds (saltern), and reclamation were extracted. The detailed process can be found in Figure 2.

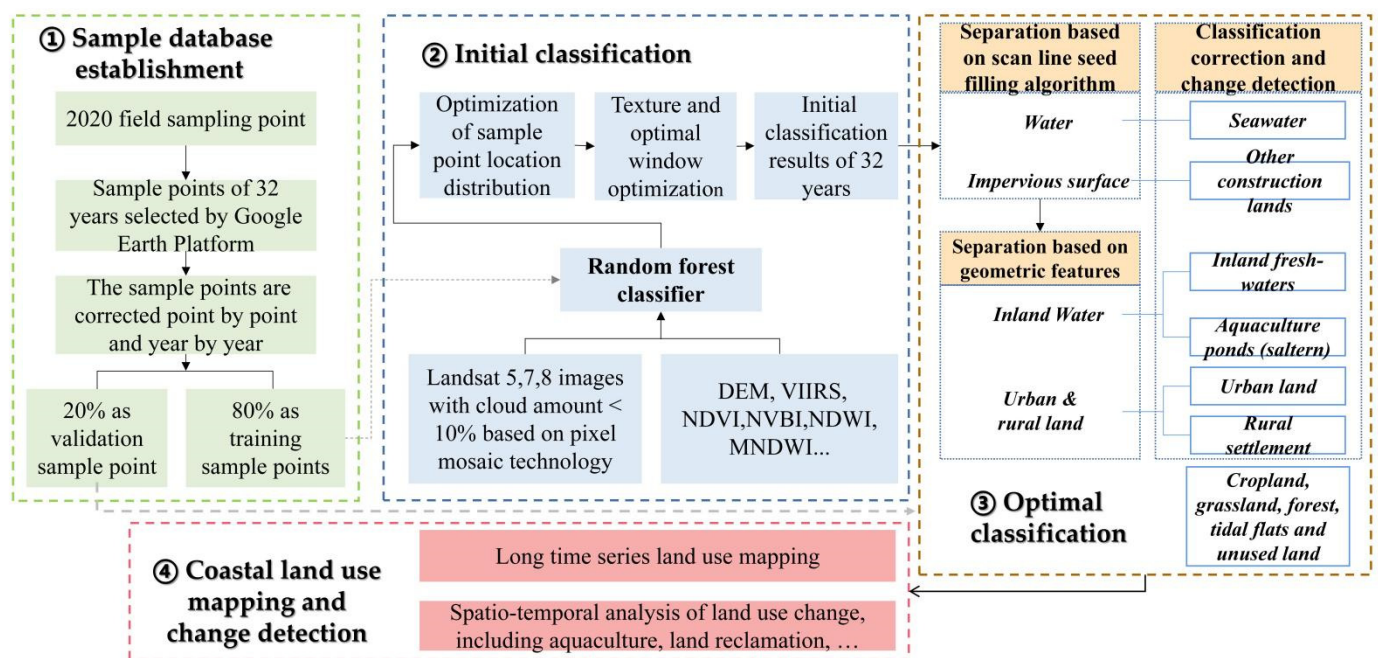


Figure 2. Flowchart of the framework for the long time-series mapping and change detection of coastal zone land use based on GEE and multi-source data fusion.

3.1. Initial Classification Based on Random Forest

We used random forest to classify the land use into cropland, impervious surface, water, forest, grassland, and other lands. To ensure the quality of input images, we optimized the distribution, texture feature extraction, and window size of input samples for each year [48]. The input samples aimed to be optimal with the highest accuracy ensured by random distribution tests. After many years of testing, the average maximum accuracy difference was up to 5.32%. For texture feature extraction, we introduced MNDWI to improve the recognition rate of water bodies and combined multi-texture features provided by GEE [49,50]. The window size for texture features was dynamically selected as 1–9 for each texture feature. There were three selected features of dissimilarity, inertia, and inverse differential moment that performed better in the multi-year results, and the optimal window size was mostly 3–5. Through the above optimization steps, we aimed to obtain

better classification results for the first level of land classes and provide a good database for subsequent processing.

3.2. Optimal Classification Method Based on Spatio-Temporal Logic

With spatial morphology, we used the scan line seed filling algorithm to distinguish city and rural settlements from impervious surfaces, and distinguish inland water and seawater from water. The inland water was further divided into inland fresh-waters and coastal aquaculture ponds (saltern) using geometric features. We then used temporal change logic and spatial distribution probability to adjust the classification and detect change for each year.

(1) Spatial morphology: the scan line seed filling algorithm

The scan line seed filling algorithm used the advantage of boundaries between seawater and inland water. These boundaries include the shore embankments for rivers and lakes, and enclosure dams for aquaculture ponds (saltern). Similar boundaries also exist between city and rural settlements because of space isolation distance. This means within the boundary, the same land-use types connect to each other. Therefore, we selected starting seed points ($seed_i$) for every urban land and rural settlement in $m \times n$ images, then assigned each starting point with coordinates (x_i, y_i) and then stacked them. For each point, we filled the corresponding area by visiting all column pixels ($A_{(x_i, y_i \pm n)}$) of the x_i line until a boundary or all pixels were visited. In this case, we moved to the next line $x_i \pm 1$, filled the new starting point $(x_i \pm 1, y_i \pm 1)$ into the stack, and repeated the above steps (Algorithm 1 lines 2–5) until the stack was empty, leading to the image result A .

Next, we distinguished aquaculture ponds (saltern) from inland water, which includes inland fresh-waters. Unlike inland fresh-waters, aquaculture ponds (saltern) always have regular shapes. We calculated three geometric features to distinguish them: centerline length L_i , aspect ratio R_i , and convexity $Conv_i$, where L_i is the sum of C_i , which is the median value of the left and right contour boundaries of the target P_i , R_i is the ratio of L_i to the total number of pixels S_i , and $Conv_i$ is the ratio of the convex perimeter $P_{i(c)}$ and the perimeter $P_{i(p)}$ ratio [51].

$$C_i = \frac{P_{i(left)} + P_{i(right)}}{2} \quad (1)$$

$$L_i = \sum_{i=1}^n C_i \quad (2)$$

$$R_i = \frac{L_i}{S_i} \quad (3)$$

$$Conv_i = \frac{P_{i(c)}}{P_{i(p)}} \quad (4)$$

Aquaculture ponds (saltern) are featured as smaller L_i , R_i and larger $Conv_i$ compared to inland fresh-waters. We identified the water bodies as aquaculture ponds (saltern) when and only when the three geometric features met the thresholds at the same time in order to avoid misclassifying broken rivers (Algorithm 1 lines 10–12). Before doing this, we binarized the image A as 0 or 1 from the last step to obtain individual water bodies $B_{(1,2,\dots,i)}$ and the respective boundaries $P_{(1,2,\dots,i)}$ through eight-neighborhood elimination (Algorithm 1 lines 7–9).

(2) Classification correction and change detection

Some stable land-use types may change a lot in the long-term and high-frequency mapping data because of classification errors. Artificial land-use types such as aquaculture ponds (saltern), impervious surface, and cropland usually remain stable, which means it is impossible for them to change frequently. Based on this logic, we used a bi-directional spatio-temporal logical consistency algorithm to adjust classification results, which is based mainly on the probability of distribution of land-use types, Algorithm 1 lines 13–17, where W denotes the time-series data constructed from $B_{1987} - B_{2020}$, W_s is the seed window,

W_d is the detection window, W_a, W_b are the start and end windows, respectively, K_s is the land-use type of the seed window, K_d is the dominant land-use type in the detection window, $prob$ is the distribution probability of a land-use type in the detection window, $count(W_a = W_b)$ gives the number of consistent land-use types, and Γ denotes the final results. For bi-direction, we checked if K_s was consistent with K_d or not. If consistent, the pixel $\Gamma_{b+1} - \Gamma_{b+d}$ in the detection window was adjusted for K_d , and the seed window moved forward/back to the end/beginning of the detection window. Otherwise, the seed window moved forward/back one position to $s \pm 1$, and we checked whether K_s was consistent with K_d or not again. Here, we determined the dominant land-use type using a threshold of 0.6 for distribution probability.

Algorithm 1. The whole Algorithm is as follows, A, B, Γ respectively representing the output image results of different steps.

```

/* step1: Separation of impervious surface (city, rural settlement, and construction land) and
water (inland fresh-waters, aquaculture ponds (saltern) and seawater) based on scan line seed */
1. stack  $\leftarrow []$ , seedi  $\leftarrow (x_i, y_i)$ ,  $i \leftarrow 1, x, y \in (m, n)$ 
2. repeat
3. if  $A_{(x_i, y_i \pm n)} \neq 0$  then  $A_{(x_i, y_i \pm n)}$  is true
4. else  $x_i \pm 1$ 
5. stack  $\leftarrow [(x_i \pm 1, y_i \pm 1), \dots, (x_i \pm 1, y_i \pm n)]$ 
6. Until stack is null
/* step2: Separation of inland fresh-waters and aquaculture ponds (saltern) based on spatial
morphology */
7. if  $A > \sigma = 1$  else = 0
8.  $B_{(1,2,\dots,i)} \leftarrow A$ 
9.  $P_{(1,2,\dots,i)} \leftarrow$  the 8-connectivity neighborhood outlines  $B_{(1,2,\dots,i)}$ 
10.  $C_i \leftarrow \frac{P_{i(left)} + P_{i(right)}}{2}$ 
11.  $L_i \leftarrow \sum_{i=1}^n C_i$ ,  $R_i \leftarrow \frac{L_i}{S_i}$ ,  $Conv_i \leftarrow \frac{P_{i(c)}}{P_{i(p)}}$ 
12. if  $count(L_i + R_i + Conv_i) = 3$  then  $P_i$  is true
/* bi-directional spatio-temporal logical consistency check */
13.  $W \leftarrow (B_{1987} - B_{2020})$ 
14.  $prob \leftarrow \frac{\sum_{d=b+1}^{a=b+d} count(W_a=W_b)}{W_d}$ 
15. If  $prob_{W_d} \geq 0.6$  and  $W_s = K_d$ , then  $\Gamma_{b+1} - \Gamma_{b+d} = K_s$ ,  $s \leftarrow a$ 
16. If  $prob_{W_d} \geq 0.6$  and  $W_s \neq K_d$ , then  $s = s + 1$ 
17. End

```

4. Results

4.1. Land Use Classification and Accuracy

We classified the land use in the Bohai rim coastal area for each year from 1987 to 2020 (Figure 3a). Results show that, in 1987, the study area was dominated by cropland (105,463.5 km²), accounting for 53.97% of the total area. This was followed by seawater (23.66%) and unused land (8.24%). Despite its dominance, the area of cropland has decreased sharply in the past three decades, from 53.97% to 37.41%. A similar observation was made for unused land. Most of the lost cropland was transformed into rural settlements, city, and construction land (e.g., ports), accounting for 19.21% of the cropland in 1987 (Table 2). For transformed unused land, compared to 1987, 34.84% became grassland and 50.05% became forest. This indicates an increasing effort spent by the Bohai rim coastal area on ecological protection and restoration. However, seawater also decreased, which illustrates the expansion of coastal land areas used for aquaculture ponds (saltern), industrial, mining, and harbors, showing the prominent aquaculture and land reclamation in this area.

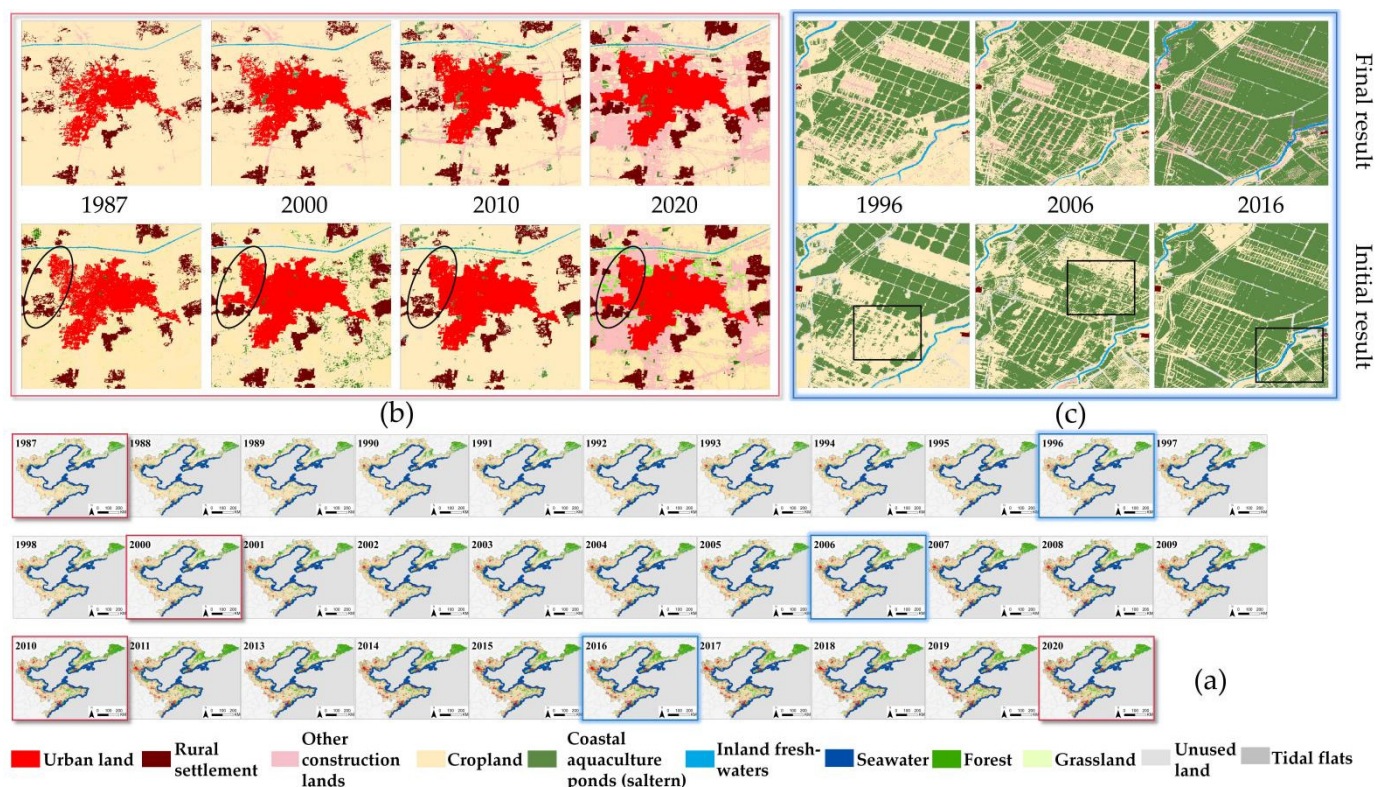


Figure 3. Long-term time series mapping result of Bohai rim coastal area: (a) results of annual classification; (b) comparison of the results of urban land expansion; (c) comparison of the results of aquaculture ponds (saltern) in different years.

Table 2. Transfer matrix of land use change in Bohai rim coastal area from 1987 to 2020.

1987 \ 2020	CRP	GRS	FRT	APS	UBL	UUS	IFW	TDF	RST	CIT	SWT
	CRP	66.59	2.28	5.07	4.72	9.46	0.80	0.56	0.25	6.49	3.25
GRS	16.02	36.60	43.08	0.27	1.04	1.47	0.10	0.14	0.63	0.65	0.00
FRT	1.11	7.28	90.47	0.09	0.15	0.62	0.01	0.06	0.07	0.13	0.00
APS	22.37	1.20	6.40	43.80	16.80	0.92	0.51	0.39	2.21	4.27	1.13
UBL	0.00	0.00	0.00	0.00	100.00	0.00	0.00	0.00	0.00	0.00	0.00
UUS	8.06	34.84	50.05	0.51	0.64	4.07	0.56	0.00	0.64	0.61	0.02
IFW	3.99	0.22	2.63	0.70	1.51	0.55	88.37	0.01	0.32	0.38	1.32
TDF	4.26	19.72	40.93	1.30	5.03	0.00	0.07	20.72	2.50	3.86	1.60
RST	0.00	0.00	0.00	0.00	0.00	0.00	0.00	0.00	78.78	21.22	0.00
CIT	0.00	0.00	0.00	0.00	0.00	0.00	0.00	0.00	0.00	99.99	0.01
SWT	0.84	0.04	0.09	2.59	2.60	0.00	0.02	0.51	0.06	0.27	92.96

Note: CRP denotes cropland, GRS denotes grassland, FRT denotes forest, APS denotes coastal aquaculture ponds (saltern), SWT denotes seawater, IFW denotes inland fresh-waters, UBL denotes urban land, RST denotes rural settlement, CTR denotes construction land, TDF denotes tidal flats, UUS denotes unused land. Units: %.

Our land use classification from 1987 to 2020 achieved an average overall accuracy (OA) of 82.30% (76.70–85.60%) and a kappa coefficient of 0.74–0.83. The recognition accuracy of rural settlements, cropland, and forest ranked in the top, with a correct rate of 91.83%, 87.90%, and 80.59%, and average completeness rate of 90.94%, 94.13%, and 84.53%, respectively. We achieved a low accuracy for mudflats (55.42%) because of a rapid increase in construction and aquaculture on mudflats, leading to significant disturbance to the spectrum in a short time, especially from 2003 to 2009. The recognition accuracy of cropland, aquaculture ponds (saltern), and impervious surface (urban land, rural settlements, and other construction lands) are higher and more stable, with the average correct

rate of 87.90%, 76.82%, and 81.29%, and the average completeness rate of 94.13%, 80.73%, and 80.89%, respectively. Here, the completeness rate is the ratio of the number of pixels obtained by a certain land type classification to the total number of actual pixels of the land type, corresponding to the missing points; the correct rate is the number of pixels correctly classified, and the actual number of land types. The ratio of the total number of pixels corresponds to the misclassification.

4.2. Land Reclamation and Aquaculture Changes

To gain a better understanding of how sea and land interact with each other, we analyzed the long-term changes of land reclamation and aquaculture (Figure 4). Land reclamation increased significantly from 1987 to 2020. The changes in land reclamation can be divided into three stages: 1987–2003, 2004–2013, 2014–2020. In the first stage, land reclamation increased slowly with an overall less than 150 km². In the second stage, land reclamation increased much faster than before with an average annual increase of 271.24 km². In the third stage, the speed of land reclamation slowed down again because of the policy control. Land reclamation was concentrated in Bohai Bay, Laizhou Bay, Liaoning Bay, and Dalian City coast (Figure 5I).

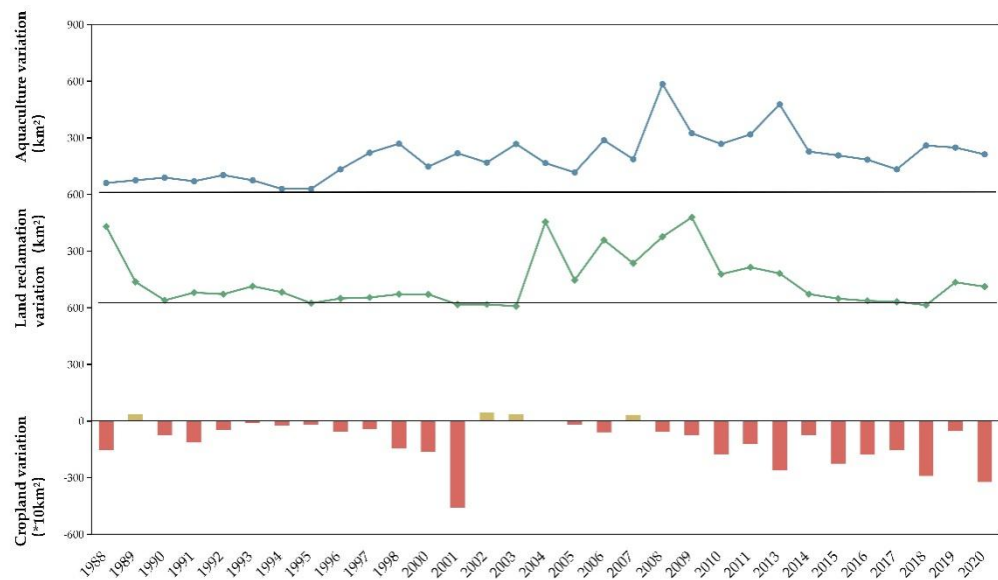


Figure 4. Analysis of the change process of a typical feature area in Bohai rim coastal area from 1987 to 2020.

Aquaculture ponds (saltern) increased by 7457.76 km² in Bohai rim coastal area from 1987 to 2020. The increase in aquaculture ponds (saltern) during 1987–1995 was low, with an average annual increase of 66.58 km². From 1996 onwards, the increase in aquaculture ponds began to show a clear upward trend, with an average annual increase of 198.36 km². These aquaculture ponds were concentrated in Bohai Bay and Laizhou Bay, especially in Binzhou, Dongying, and Weifang in Shandong. Although Shandong Province is a largely agricultural province in China, the area of cropland in Shandong has shown a decreasing trend over the past two decades. Our results show that some of the cropland has been converted into aquaculture ponds (saltern) (Figure 5II).

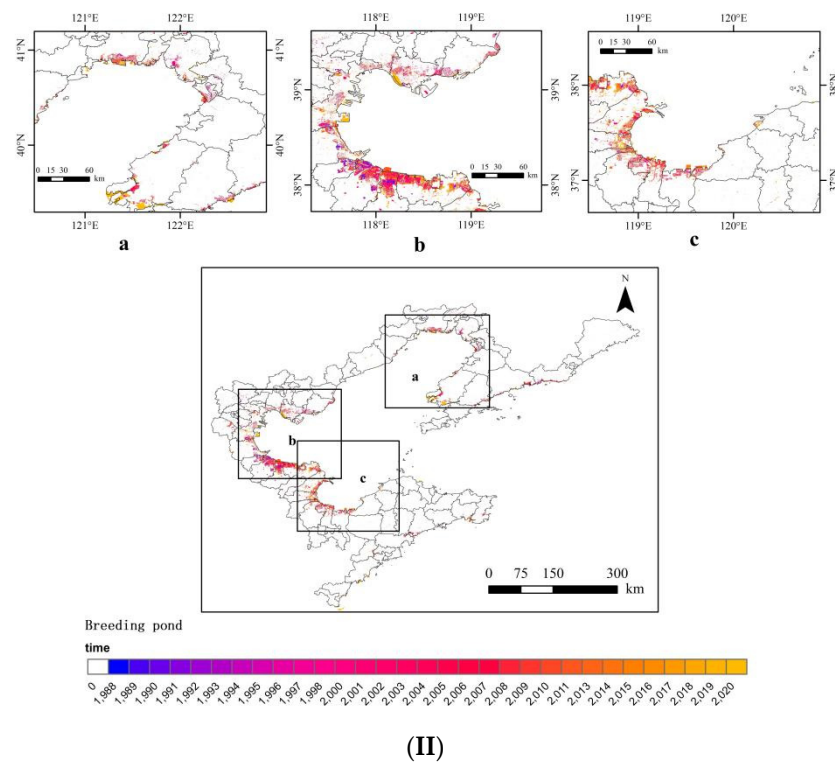
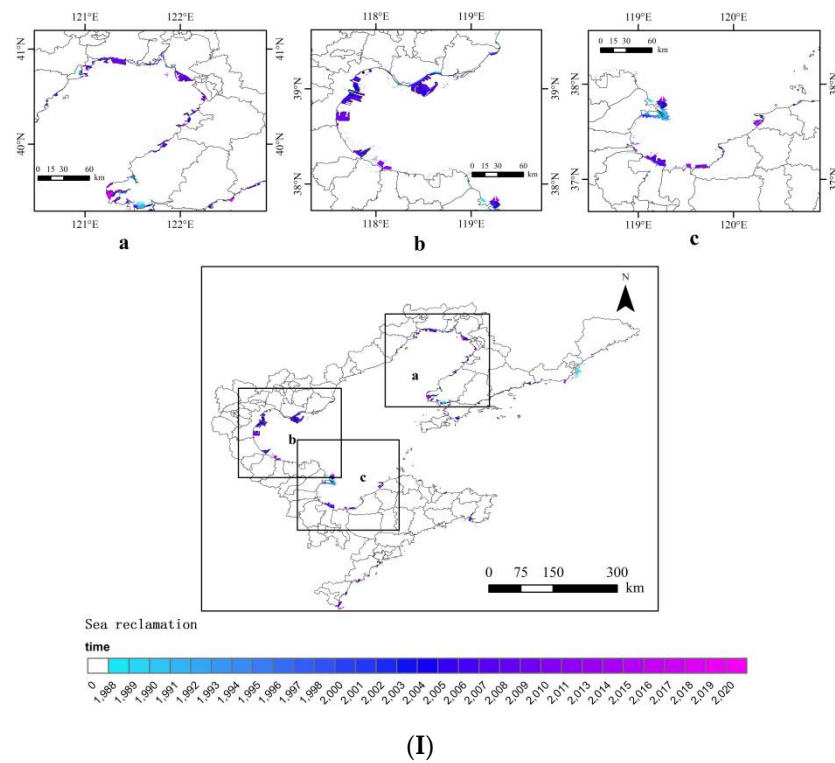


Figure 5. Mapping results of long-term land reclamation (I) and aquaculture (II).

5. Discussion

In this study, we used multi-source data fusion and prior knowledge to improve land use classification, which addresses the limitation of existing classification relying only on spectral information of features. Multi-source data fusion and prior knowledge can combine spatial neighborhood features with temporal dimensional logical features and significantly reduce the computational cost for long-term time series and high-frequency

land use classification and change detections [52]. Although some algorithms such as deep learning can achieve good recognition results for specific targets (e.g., aquaculture net cages and mudflats) [29,53], they still cannot cope with the phenomenon of “same-spectrum dissimilarity”. Some discussions are given below.

(1) Compared with previous studies, our results achieve good consistency. For example, our results show a similar land use classification system in Bohai rim coastal area with Liu [42]. The land reclamation changes found by this study are similar to Huang [33], where it was shown that coastal land reclamations were stable from 2000 to 2005 and increased rapidly from 2005 to 2010. Our research further found that the two important time points for reclamation changes are 2003 and 2013. If the time sequence is divided into three phases, the overall trend is the same: stable growth–surge growth–stable growth. We also obtained a similar distribution of land use along the landward direction with Ding [44], where it was shown that land uses near the coastline and inland boundary have relatively stable sequential positions along the landward direction, while the intermediate land uses have dynamic sequential positions leading to multiple CLUSPs. Using spatio-temporal change logic to adjust land use classification helps to improve accuracy. After the change logic correction, we found that the average overall accuracy of the corrected results improved by about 8.03%, especially for impervious surfaces and aquaculture ponds (saltern). This is because for long-term high-frequency land use mapping, classification errors may lead to unsteady classifications. In this case, using the spatio-temporal change logic to adjust frequent changes in stable land use can improve the classification accuracy and keep the actual land use changes at the same time [52]. As shown in Figure 3b, the rural settlements in the black box were divided into urban land in 2000, which is not in line with normal logic, and the final result shows a natural trend of urban expansion. Final result in Figure 3c, the identification rate of aquaculture ponds (saltern) in the black box is higher and the details are better.

(2) There are some uncertainties in our results. By analyzing the results of image classification in previous years, we can find that the classification accuracy tends to be low with earlier years. For example, the overall accuracies of 1987, 1988, 1993, and 1994 were 79.31%, 79.85%, 76.70%, and 77.55%, respectively. Since 1997, the accuracy has been more than 80% year by year, and the average OA from 1997 to 2020 is 84.35%. On the one hand, the accuracy of the classification was directly affected by the generally poor imaging quality in earlier years. On the other hand, the lack of high-resolution image-assisted discrimination before 2000, relying only on visual identification and empirical judgment, led to poor quality of sample points as well. Furthermore, some special land-cover types in the coastal zone, such as mudflats, have extremely unstable spatial distribution due to the direct influence of tides and the rapid land-use changes, resulting in the introduction of large uncertainties in the sample point selection. For example, 30% of mudflats were misclassified during fast-growing land reclamation (2004–2009). In addition, during the segmentation under medium-resolution images, aquaculture ponds (saltern) may be misclassified as a river because the boundary between aquaculture ponds (saltern) and rivers may be only a few meters wide. Another uncertainty comes when urban land and rural settlements are connected by main roads. In this situation, some rural settlements close to urban land would be misclassified as urban land in advance.

(3) The above uncertainties can be reduced by using high-resolution satellite data such as LiDAR data, which provide special backscatter responses to water and hardened surfaces, which is helpful to distinguish between water bodies and impermeable surfaces [54,55]. In this study, we did not differentiate saltern from aquaculture ponds, because there is a little difference in morphology and spectra between aquaculture ponds and saltern. It is expected that in the follow-up research, a hyperspectral and water color analysis will be used to realize the separation of the two.

6. Conclusions

In this paper, we proposed a method to map the long-term land-use changes in the Bohai rim coastal area. We first refined the classification system to include aquaculture and land reclamation to consider coastal characteristics. Then, we applied multi-source data fusion, the random forest algorithm, the optimal classification method using spatial morphology and temporal change logic to make it computationally possible to map the long-term annual time-series and detect changes in the Bohai rim coastal area from 1987 to 2020. Validation showed an overall acceptable error, which illustrates the use of multi-source data fusion and prior knowledge to distinguish land use classes with similar spectra. We found two key years for aquaculture and land reclamation, before and after which the changes in respective land use are different. The proposed method shows its strength in the land use classification for coastal zones. This method is transferable to land use mapping for coastal zones, especially for long-term time series and high-frequency mapping.

Author Contributions: Conceptualization, D.C., Y.W. and Z.S.; formal analysis, D.C., Y.W. and J.L.; funding acquisition, Y.W.; methodology, Y.W. and Z.S.; writing—original draft, D.C., Y.W., Z.S. and J.L.; writing—review and editing, D.C., Y.W., Z.S., J.C. and S.S. All authors have read and agreed to the published version of the manuscript.

Funding: This research was funded by the National Natural Science Foundation of China (No.42001131).

Acknowledgments: We appreciate the critical and constructive comments and suggestions from the reviewers that helped improve the quality of this manuscript.

Conflicts of Interest: The authors declare no conflict of interest.

References

1. Chuai, X.; Wen, J.; Zhuang, D.; Guo, X.; Yuan, Y.; Lu, Y.; Zhang, M.; Li, J. Intersection of Physical and Anthropogenic Effects on Land-Use/Land-Cover Changes in Coastal China of Jiangsu Province. *Sustainability* **2019**, *11*, 2370. [[CrossRef](#)]
2. Tian, B.; Wu, W.; Yang, Z.; Zhou, Y. Drivers, trends, and potential impacts of long-term coastal reclamation in China from 1985 to 2010. *Estuarine Coast. Shelf Sci.* **2016**, *170*, 83–90. [[CrossRef](#)]
3. Wang, D.; Chen, W.; Wei, W.; Bird, B.W.; Zhang, L.; Sang, M.; Wang, Q. Research on the Relationship between Urban Development Intensity and Eco-Environmental Stresses in Bohai Rim Coastal Area, China. *Sustainability* **2016**, *8*, 406. [[CrossRef](#)]
4. Zong, S.; Hu, Y.; Zhang, Y.; Wang, W. Identification of land use conflicts in China's coastal zones: From the perspective of ecological security. *Ocean Coast. Manag.* **2021**, *213*, 105841. [[CrossRef](#)]
5. Zou, L.; Liu, Y.; Wang, J.; Yang, Y.; Wang, Y. Land use conflict identification and sustainable development scenario simulation on China's southeast coast. *J. Clean. Prod.* **2019**, *238*, 117899. [[CrossRef](#)]
6. Yasir, M.; Hui, S.; Binghu, H.; Rahman, S.U. Coastline extraction and land use change analysis using remote sensing (RS) and geographic information system (GIS) technology—A review of the literature. *Rev. Environ. Health* **2020**, *35*, 453–460. [[CrossRef](#)]
7. Camilleri, S.; De Giglio, M.; Stecchi, F.; Pérez-Hurtado, A. Land use and land cover change analysis in predominantly man-made coastal wetlands: Towards a methodological framework. *Wetl. Ecol. Manag.* **2017**, *25*, 23–43. [[CrossRef](#)]
8. Liu, C.; Yang, M.; Hou, Y.; Xue, X. Ecosystem service multifunctionality assessment and coupling coordination analysis with land use and land cover change in China's coastal zones. *Sci. Total Environ.* **2021**, *797*, 149033. [[CrossRef](#)] [[PubMed](#)]
9. Tian, Y.; Zhou, D.; Jiang, G. Conflict or Coordination? Multiscale assessment of the spatio-temporal coupling relationship between urbanization and ecosystem services: The case of the Jingjinji Region, China. *Ecol. Indic.* **2020**, *117*, 106543. [[CrossRef](#)]
10. Coppin, P.R.; Bauer, M.E. Digital change detection in forest ecosystems with remote sensing imagery. *Remote Sens. Rev.* **1996**, *13*, 207–234. [[CrossRef](#)]
11. Mountrakis, G.; Im, J.; Ogole, C. Support vector machines in remote sensing: A review. *ISPRS J. Photogramm. Remote Sens.* **2011**, *66*, 247–259. [[CrossRef](#)]
12. Schneider, A. Monitoring land cover change in urban and peri-urban areas using dense time stacks of Landsat satellite data and a data mining approach. *Remote Sens. Environ.* **2012**, *124*, 689–704. [[CrossRef](#)]
13. Xie, S.; Liu, L.; Zhang, X.; Yang, J.; Chen, X.; Gao, Y. Automatic Land-Cover Mapping using Landsat Time-Series Data based on Google Earth Engine. *Remote Sens.* **2019**, *11*, 3023. [[CrossRef](#)]
14. Vali, A.; Comai, S.; Matteucci, M. Deep Learning for Land Use and Land Cover Classification based on Hyperspectral and Multispectral Earth Observation Data: A Review. *Remote Sens.* **2020**, *12*, 2495. [[CrossRef](#)]
15. Jin, Y.; Liu, X.; Yao, J.; Zhang, X.; Zhang, H. Mapping the annual dynamics of cultivated land in typical area of the Middle-lower Yangtze plain using long time-series of Landsat images based on Google Earth Engine. *Int. J. Remote Sens.* **2019**, *41*, 1625–1644. [[CrossRef](#)]

16. Grings, F.; Roitberg, E.; Barraza, V. EVI Time-Series Breakpoint Detection Using Convolutional Networks for Online Deforestation Monitoring in Chaco Forest. *IEEE Trans. Geosci. Remote Sens.* **2019**, *58*, 1303–1312. [[CrossRef](#)]
17. Verbesselt, J.; Hyndman, R.; Newnham, G.; Culvenor, D. Detecting trend and seasonal changes in satellite image time series. *Remote Sens. Environ.* **2010**, *114*, 106–115. [[CrossRef](#)]
18. Yang, Z.; Li, J.; Shen, Y.; Miao, H.; Yan, X. A denoising method for inter-annual NDVI time series derived from Landsat images. *Int. J. Remote Sens.* **2018**, *39*, 3816–3827. [[CrossRef](#)]
19. Gorelick, N.; Hancher, M.; Dixon, M.; Ilyushchenko, S.; Thau, D.; Moore, R. Google Earth Engine: Planetary-scale geospatial analysis for everyone. *Remote Sens. Environ.* **2017**, *202*, 18–27. [[CrossRef](#)]
20. Wang, X.; Xiao, X.; Zou, Z.; Chen, B.; Ma, J.; Dong, J.; Doughty, R.B.; Zhong, Q.; Qin, Y.; Dai, S.; et al. Tracking annual changes of coastal tidal flats in China during 1986–2016 through analyses of Landsat images with Google Earth Engine. *Remote Sens. Environ.* **2020**, *238*, 110987. [[CrossRef](#)] [[PubMed](#)]
21. Zhang, K.; Dong, X.; Liu, Z.; Gao, W.; Hu, Z.; Wu, G. Mapping Tidal Flats with Landsat 8 Images and Google Earth Engine: A Case Study of the China's Eastern Coastal Zone circa 2015. *Remote Sens.* **2019**, *11*, 924. [[CrossRef](#)]
22. Badamfirooz, J.; Mousazadeh, R. Quantitative assessment of land use/land cover changes on the value of ecosystem services in the coastal landscape of Anzali International Wetland. *Environ. Monit. Assess.* **2019**, *191*, 694. [[CrossRef](#)]
23. Gao, Y.; Cui, L.; Liu, J.; Li, W.; Lei, Y. China's coastal-wetland change analysis based on high-resolution remote sensing. *Mar. Freshw. Res.* **2020**, *71*, 1161–1181. [[CrossRef](#)]
24. Veettil, B.K.; Quang, N.X. Mangrove forests of Cambodia: Recent changes and future threats. *Ocean Coast. Manag.* **2019**, *181*, 181. [[CrossRef](#)]
25. Ma, C.; Ai, B.; Zhao, J.; Xu, X.; Huang, W. Change Detection of Mangrove Forests in Coastal Guangdong during the Past Three Decades Based on Remote Sensing Data. *Remote Sens.* **2019**, *11*, 921. [[CrossRef](#)]
26. Fu, Y.; Guo, Q.; Wu, X.; Fang, H.; Pan, Y. Analysis and Prediction of Changes in Coastline Morphology in the Bohai Sea, China, Using Remote Sensing. *Sustainability* **2017**, *9*, 900. [[CrossRef](#)]
27. Wang, Y.; Hou, X.; Shi, P.; Yu, L. Detecting Shoreline Changes in Typical Coastal Wetlands of Bohai Rim in North China. *Wetlands* **2013**, *33*, 617–629. [[CrossRef](#)]
28. Xu, N.; Gao, Z.; Ning, J. Analysis of the characteristics and causes of coastline variation in the Bohai Rim (1980–2010). *Environ. Earth Sci.* **2016**, *75*, 1–11. [[CrossRef](#)]
29. Fu, Y.; Deng, J.; Wang, H.; Comber, A.; Yang, W.; Wu, W.; You, S.; Lin, Y.; Wang, K. A new satellite-derived dataset for marine aquaculture areas in China's coastal region. *Earth Syst. Sci. Data* **2021**, *13*, 1829–1842. [[CrossRef](#)]
30. Duan, Y.; Li, X.; Zhang, L.; Liu, W.; Liu, S.; Chen, D.; Ji, H. Detecting spatiotemporal changes of large-scale aquaculture ponds regions over 1988–2018 in Jiangsu Province, China using Google Earth Engine. *Ocean Coast. Manag.* **2020**, *188*, 105144. [[CrossRef](#)]
31. Sun, S.; Zhang, Y.; Song, Z.; Chen, B.; Zhang, Y.; Yuan, W.; Chen, C.; Chen, W.; Ran, X.; Wang, Y. Mapping Coastal Wetlands of the Bohai Rim at a Spatial Resolution of 10 m Using Multiple Open-Access Satellite Data and Terrain Indices. *Remote Sens.* **2020**, *12*, 4114. [[CrossRef](#)]
32. Xia, Z.; Guo, X.; Chen, R. Automatic extraction of aquaculture ponds based on Google Earth Engine. *Ocean Coast. Manag.* **2020**, *198*, 105348. [[CrossRef](#)]
33. Huang, C.; Zhang, C.; Liu, Q.; Wang, Z.; Li, H.; Liu, G. Land reclamation and risk assessment in the coastal zone of China from 2000 to 2010. *Reg. Stud. Mar. Sci.* **2020**, *39*, 101422. [[CrossRef](#)]
34. Sengupta, D.; Chen, R.; Meadows, M.E.; Choi, Y.R.; Banerjee, A.; Zilong, X. Mapping Trajectories of Coastal Land Reclamation in Nine Deltaic Megacities using Google Earth Engine. *Remote Sens.* **2019**, *11*, 2621. [[CrossRef](#)]
35. Chen, J.; Chen, J.; Liao, A.; Cao, X.; Chen, L.; Chen, X.; He, C.; Han, G.; Peng, S.; Lu, M.; et al. Global land cover mapping at 30 m resolution: A POK-based operational approach. *ISPRS J. Photogramm. Remote Sens.* **2015**, *103*, 7–27. [[CrossRef](#)]
36. Gong, P.; Wang, J.; Yu, L.; Zhao, Y.; Zhao, Y.; Liang, L.; Niu, Z.; Huang, X.; Fu, H.; Liu, S.; et al. Finer resolution observation and monitoring of global land cover: First mapping results with Landsat TM and ETM+ data. *Int. J. Remote Sens.* **2012**, *34*, 2607–2654. [[CrossRef](#)]
37. Sun, Z.; Luo, J.; Yang, J.; Yu, Q.; Zhang, L.; Xue, K.; Lu, L. Nation-Scale Mapping of Coastal Aquaculture Ponds with Sentinel-1 SAR Data Using Google Earth Engine. *Remote Sens.* **2020**, *12*, 3086. [[CrossRef](#)]
38. Virdis, S.G.P. An object-based image analysis approach for aquaculture ponds precise mapping and monitoring: A case study of Tam Giang-Cau Hai Lagoon, Vietnam. *Environ. Monit. Assess.* **2014**, *186*, 117–133. [[CrossRef](#)]
39. Cheng, B.; Liang, C.; Liu, X.; Liu, Y.; Ma, X.; Wang, G. Research on a novel extraction method using Deep Learning based on GF-2 images for aquaculture areas. *Int. J. Remote Sens.* **2020**, *41*, 3575–3591. [[CrossRef](#)]
40. Han, X.; Chen, X.; Feng, L. Four decades of winter wetland changes in Poyang Lake based on Landsat observations between 1973 and 2013. *Remote Sens. Environ.* **2015**, *156*, 426–437. [[CrossRef](#)]
41. Sheng, Y.; Song, C.; Wang, J.; Lyons, E.; Knox, B.R.; Cox, J.S.; Gao, F. Representative lake water extent mapping at continental scales using multi-temporal Landsat-8 imagery. *Remote Sens. Environ.* **2016**, *185*, 129–141. [[CrossRef](#)]
42. Liu, Y.; Hou, X.; Li, X.; Song, B.; Wang, C. Assessing and predicting changes in ecosystem service values based on land use/cover change in the Bohai Rim coastal zone. *Ecol. Indic.* **2020**, *111*, 106004. [[CrossRef](#)]
43. Zhang, Y.; Zhao, L.; Liu, J.; Liu, Y.; Li, C. The Impact of Land Cover Change on Ecosystem Service Values in Urban Agglomerations along the Coast of the Bohai Rim, China. *Sustainability* **2015**, *7*, 10365–10387. [[CrossRef](#)]

44. Ding, Z.; Su, F.; Zhang, J.; Zhang, Y.; Luo, S.; Tang, X. Clustering Coastal Land Use Sequence Patterns along the Sea–Land Direction: A Case Study in the Coastal Zone of Bohai Bay and the Yellow River Delta, China. *Remote Sens.* **2019**, *11*, 2024. [[CrossRef](#)]
45. Li, H.; Wan, W.; Fang, Y.; Zhu, S.; Chen, X.; Liu, B.; Hong, Y. A Google Earth Engine-enabled software for efficiently generating high-quality user-ready Landsat mosaic images. *Environ. Model. Softw.* **2019**, *112*, 16–22. [[CrossRef](#)]
46. Jiang, H.; Feng, M.; Zhu, Y.; Lu, N.; Huang, J.; Xiao, T. An Automated Method for Extracting Rivers and Lakes from Landsat Imagery. *Remote Sens.* **2014**, *6*, 5067–5089. [[CrossRef](#)]
47. Zeng, Z.; Wang, D.; Tan, W.; Huang, J. Extracting aquaculture ponds from natural water surfaces around inland lakes on medium resolution multispectral images. *Int. J. Appl. Earth Obs. Geoinf.* **2019**, *80*, 13–25. [[CrossRef](#)]
48. Heydari, S.S.; Mountrakis, G. Effect of classifier selection, reference sample size, reference class distribution and scene heterogeneity in per-pixel classification accuracy using 26 Landsat sites. *Remote Sens. Environ.* **2018**, *204*, 648–658. [[CrossRef](#)]
49. Feyisa, G.L.; Meilby, H.; Fensholt, R.; Proud, S.R. Automated Water Extraction Index: A new technique for surface water mapping using Landsat imagery. *Remote Sens. Environ.* **2014**, *140*, 23–35. [[CrossRef](#)]
50. Zhou, Y.; Dong, J.; Xiao, X.; Xiao, T.; Yang, Z.; Zhao, G.; Zou, Z.; Qin, Y. Open Surface Water Mapping Algorithms: A Comparison of Water-Related Spectral Indices and Sensors. *Water* **2017**, *9*, 256. [[CrossRef](#)]
51. Van Der Werff, H.; Van Der Meer, F. Shape-based classification of spectrally identical objects. *ISPRS J. Photogramm. Remote Sens.* **2008**, *63*, 251–258. [[CrossRef](#)]
52. Li, X.; Gong, P.; Liang, L. A 30-year (1984–2013) record of annual urban dynamics of Beijing City derived from Landsat data. *Remote Sens. Environ.* **2015**, *166*, 78–90. [[CrossRef](#)]
53. Wang, X.; Xiao, X.; Zou, Z.; Hou, L.; Qin, Y.; Dong, J.; Doughty, R.B.; Chen, B.; Zhang, X.; Chen, Y.; et al. Mapping coastal wetlands of China using time series Landsat images in 2018 and Google Earth Engine. *ISPRS J. Photogramm. Remote Sens.* **2020**, *163*, 312–326. [[CrossRef](#)] [[PubMed](#)]
54. Kim, H.; Lee, S.B.; Min, K.S. Shoreline Change Analysis using Airborne LiDAR Bathymetry for Coastal Monitoring. *J. Coast. Res.* **2017**, *79*, 269–273. [[CrossRef](#)]
55. Ottinger, M.; Clauss, K.; Kuenzer, C. Aquaculture: Relevance, distribution, impacts and spatial assessments—A review. *Ocean Coast. Manag.* **2016**, *119*, 244–266. [[CrossRef](#)]